Original Article

DOI: 10.5582/bst.2024.01112

Establishment of nomogram prediction model of contrast-enhanced ultrasound and Gd-EOB-DTPA-enhanced MRI for vessels encapsulating tumor clusters pattern of hepatocellular carcinoma

Feiqian Wang[1,2], Kazushi Numata[2,*], Akihiro Funaoka[2], Xi Liu[3], Takafumi Kumamoto[2], Kazuhisa Takeda[2], Makoto Chuma[2], Akito Nozaki[2], Litao Ruan[1], Shin Maeda[4]

[1] Department of Ultrasound, The First Affiliated Hospital of Xi'an Jiaotong University, Xi'an, Shaanxi, China;
[2] Gastroenterological Center, Yokohama City University Medical Center, Yokohama, Kanagawa, Japan;
[3] Department of Pathology, The First Affiliated Hospital of Xi'an Jiaotong University, Xi'an, Shaanxi, China;
[4] Division of Gastroenterology, Yokohama City University Graduate School of Medicine, Yokohama, Kanagawa, Japan.

SUMMARY To establish clinical prediction models of vessels encapsulating tumor clusters (VETC) pattern using preoperative contrast-enhanced ultrasound (CEUS) and gadolinium-ethoxybenzyl-diethylenetriamine pentaacetic acid magnetic resonance imaging (EOB-MRI) in patients with hepatocellular carcinoma (HCC). A total of 111 resected HCC lesions from 101 patients were included. Preoperative imaging features of CEUS and EOB-MRI, postoperative recurrence, and survival information were collected from medical records. The best subset regression and multivariable Cox regression were used to select variables to establish the prediction model. The VETC-positive group had a statistically lower survival rate than the VETC-negative group. The selected variables were peritumoral enhancement in the arterial phase (AP), hepatobiliary phase (HBP) on EOB-MRI, intratumoral branching enhancement in the AP of CEUS, intratumoral hypoenhancement in the portal phase of CEUS, incomplete capsule, and tumor size. A nomogram was developed. High and low nomogram scores with a cutoff value of 168 points showed different recurrence-free survival rates and overall survival rates. The area under the curve (AUC) and accuracy were 0.804 and 0.820, respectively, indicating good discrimination. Decision curve analysis showed a good clinical net benefit (threshold probability > 5%), while the Hosmer-Lemeshow test yielded excellent calibration (P = 0.6759). The AUC of the nomogram model combining EOB-MRI and CEUS was higher than that of the models with EOB-MRI factors only (0.767) and CEUS factors only (0.7). The nomogram verified by bootstrapping showed AUC and calibration curves similar to those of the nomogram model. The Prediction model based on CEUS and EOB-MRI is effective for preoperative noninvasive diagnosis of VETC.

Keywords vessels encapsulating tumor clusters, diagnosis, hepatocellular carcinoma, contrast-enhanced ultrasound, gadolinium-ethoxybenzyl-diethylenetriamine, pentaacetic acid magnetic resonance imaging

1. Introduction

Approximately 40–70% hepatocellular carcinoma (HCC) patients suffer from postoperative recurrence within 5 years (*1*). The intrahepatic metastasis rate was 78.5%, according to an autopsy study of 240 patients with HCC in Japan (*2*). Because metastasis and recurrence of HCC can seriously affect the survival of patients, its mechanism has been extensively explored. Vessels encapsulating tumor clusters (VETC) patterns are a recently discovered tumor vascular growth pattern (*3*). VETC coating provides an "integrated ecosystem" that can protect or shield tumor cells from anoikis (apoptosis upon loss of attachment to the extracellular matrix), shearing forces in the bloodstream, and immunological attack (*3*). Thus, it has a very strong invasion potential. VETC patterns have been reported to be able to predict the response and prognosis after various treatments for HCC, including transcatheter artery chemoembolization (TACE) benefit (*4,5*), liver transplantation (*6*), and sorafenib (*7*). VETC was independently associated with early recurrence within 2 years (hazard ratio [HR]: 1.52, P = 0.023), disease-free survival (HR: 1.66, P = 0.002), and overall survival (OS) (HR: 2.26, P = 0.001)

(*8*). Currently, the diagnosis of VETC patterns can only be assessed by histopathological staining of surgically resected tissue with endothelial cell-specific markers such as cluster of differentiation (CD)34 and CD31. In addition, for patients who cannot be treated with surgical resection, a histopathology-based VETC diagnosis cannot be obtained. Therefore, it is of great clinical significance to use a modality independent of pathology to accurately diagnose VETC, especially to predict VETC before surgery.

Among all imaging modalities, contrast-enhanced ultrasound (CEUS) using Sonazoid agent and magnetic resonance imaging using gadolinium-ethoxybenzyl-diethylenetriamine penta-acetic acid (EOB-MRI) have been highlighted as breakthrough imaging modalities for HCC diagnosis (*9*). CEUS and EOB-MRI have the widely recognized advantages of nonradiation, noninvasive, good repeatability, and few side effects (*10*). The microbubbles of contrast agents are not metabolized by the liver and kidney; thus, CEUS is safer than enhanced CT and MRI for patients with poor liver and kidney function. The Japan Society of Hepatology (JSH) and European Association for the Study of the Liver (EASL) guidelines recommend EOB-MRI and CEUS as first- and second-line approaches for liver cancer diagnosis, respectively (*11,12*). Chinese guidelines recommend CEUS as a first-line examination for high-risk populations of HCC (*13*). In real-world practice, some indicators in EOB-MRI have been reported to be associated with the occurrence of VETC in patients with HCC (*14,15*). However, the reported diagnostic strategy based on MRI features is not good enough to provide a satisfactory diagnosis (pooled accuracy was 57.6–74%) (*16*). Sonazoid agents are pure blood pool microbubbles that cannot enter the stroma (*10*). Therefore, it can be used to evaluate blood perfusion and microcirculation. We previously found that EOB-MRI is more likely to miss the detection of intratumoral hypervascularity than CEUS in small lesions ($P = 0.012$), heterogeneity ($P = 0.013$), and slight enhancement in arterial phase (AP) ($P = 0.009$) (*17*). Regrettably, there is very little English literature on the application of CEUS for the preoperative diagnosis of VETC (*18,19*). By combining two or more imaging techniques, multimodal imaging is believed to enhance the diagnostic accuracy by overcoming the limitations of independent techniques and providing a large amount of information to minimize the risk of false positives or negatives (*20*). As the quality of CEUS images is easily affected by lung gas and depth of the target lesion, we considered multimodal imaging of EOB-MRI and CEUS as a way to research VETC patterns.

Therefore, the primary aim of our study was to estimate the value of preoperative multimodal imaging using CEUS and EOB-MRI for predicting VETC patterns. Compared to conventional prediction approaches, nomograms present an excellent graphical easy-to-interpret visualization; by combining patients' characteristics and statistical models constructed based on diagnostic tests, higher accuracy can be achieved, facilitating the clinical decision-making process (*21*). In order for our study to be adapted to clinical needs (individualized and easy to use), the secondary aim was to establish a clinical predictive model of VETC patterns.

2. Materials and Methods

2.1. Patients Enrollment

Between September 2007 and December 2021, 196 patients with 218 HCC lesions were enrolled in this study. The inclusion criteria were as follows: (1) adult patients (≥18 years old); (2) non-pregnancy and/or non-lactation; (3) clear pathological diagnosis of HCC; and (4) definite diagnosis of VETC pattern according to the gold standard of CD34 staining in surgical specimens. The exclusion criteria were as follows: (1) either CEUS or EOB-MRI not performed within one month before hepatectomy (N/*n* = 43/47); (2) Child-Pugh grade C (N/*n* = 12/12); (3) already treated HCC lesions (N/*n* = 13/15); (4) history of other cancers (N/*n* = 10/13); (5) poor image quality, which affected the analysis of the indicators (N/*n* = 8/8); and (6) incomplete preoperative serological data (N/*n* = 7/10). After the above screening, 101 HCC patients with 111 lesions were included in this study, including 24 VETC-positive lesions and 87 VETC-negative lesions (Figure 1). This study was approved by the Ethics Review Board (No. F220700009 on June 27, 2022) of Yokohama City University Medical Center, Japan. The requirement for informed consent was waived owing to the retrospective nature of the study.

The general baseline demographic data (including age, sex, etiology of hepatitis of patients, degree of liver fibrosis, and size of the lesion) and preoperative serological indicators (including α-fetoprotein (AFP), serum albumin (Alb), total bilirubin (T-BIL), prothrombin time (Pt), platelet counts (Plt), prothrombin induced by vitamin K absence II (PIVKA-II), and indocyanine green 15 min retention (ICG-R15)) were obtained by retrospectively searching the electronic medical record system.

2.2. Grayscale US and CEUS examination

A LOGIQ E9 US system (GE Healthcare, Milwaukee, WI, USA) equipped with native tissue harmonic grayscale imaging and CEUS functions was used. Convexes and microconvexities with frequencies of 1–6 MHz and 2–5 MHz, respectively, were used. A 0.2 mL dose of perfluorobutane microbubbles (Sonazoid®, Daiichi Sankyo, Tokyo, Japan) was injected into the antecubital vein (0.2 mL/s *via* a 24-gauge cannula, followed by 2 mL of 5% glucose). CEUS images were acquired during three contrast phases: AP, portal phase

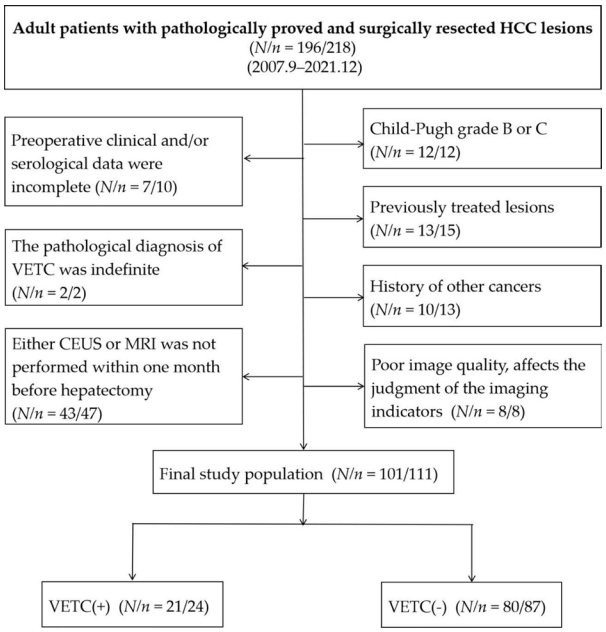

Figure 1. Flowchart of the study population. HCC: hepatocellular carcinoma; VETC: vessels encapsulating tumor clusters; CEUS: Contrast-enhanced ultrasound; EOB-MRI: Gadolinium-Ethoxybenzyl-Diethylenetriamine Penta-Acetic Acid magnetic-resonance imaging.

(PP), and postvascular phase (PVP) (10–50 and 80–120 s, and 10 min after injection, respectively). Low mechanical index mode (0.2–0.3) was used for CEUS examination.

2.3. EOB-MRI examination

MR was performed using a 1.5 T whole-body imager (Avant; Siemens Medical Systems, Erlangen, Germany). A power injector (Spectris Solaris EP; MEDRAD, Bayer Schering Pharma AG, Berlin, Germany) was used to inject 0.1 mmol/kg of Gd-EOB-DTPA (Primovist; Bayer Schering Pharma AG, Berlin, Germany) at 1 mL/s through a catheter placed in the antecubital vein, followed by flushing with 20 mL of sterile saline solution at 2 mL/s. AP, PP, late-phase, and hepatobiliary phase (HBP) scanning was performed at 25–30 s, 70–85 s, 180 s, and 20 min after initiation of the contrast injection, respectively. Images were obtained using fat-suppressed volumetric interpolated breath-hold examination (FS VIBE) T1-weighted sequences (TR, 6.2 ms; TE, 3.15 ms; flip angle, 20º; bandwidth, 260 Hz/pix; matrix, 166 × 320; acquisition time, 20 s). In addition, a fast low-angle shot (FLASH) T1-weighted sequence (TR, 115 ms; TE, 4.76 ms; flip angle, 70º; bandwidth, 260 Hz/pix; matrix, 192 × 256; acquisition time, 20 s × 3) was performed.

2.4. Interpretation of Key Imaging Features

Two doctors (F. W. and A.F., with 11 and 5 years of experience in abdominal imaging diagnosis, respectively) independently evaluated the image features of CEUS and EOB-MRI, respectively. When there were inconsistent results between the two doctors after the first image analysis, a final decision was made by an expert (K. N., with 35 years of experience in liver imaging diagnosis).

The CEUS imaging features included the following: 1) Size: the largest axial diameter on the grayscale images. If the lesion was indistinct (especially if it was isoechogenic) on the grayscale US image, size measurement on the AP or PVP of the CEUS images could be performed. 2) AP enhancement degree: hyper-/iso-enhancement (comprising more than half of the lesion area). 3) PP enhancement degree: iso-/hypo-enhancement (comprising more than half of the lesion area). 4) PVP enhancement degree: iso-/hypo-enhancement (comprising more than half of the lesion area). 5) Tumor margin (regular/irregular): "Irregular" margin is ill-defined, uneven, and/or lobulated while "regular" margin is well-defined, smooth, and round. 6) Intratumoral branching enhancement: thick or thin continuous strip-like, branching, separation-like enhancement in AP. 7) Intratumoral homogeneity: "homogeneous" enhancement was defined as a whole and diffuse enhancement of the lesion, while "heterogeneous" enhancement was defined as two or more enhancement echoes mixed enhancement of the lesion.

The EOB-MRI features included the following: 1) Intratumoral hyperenhancement in AP: high/iso- or low (compared with the background liver parenchyma). 2) Intratumoral hypoenhancement in HBP: low/iso- or high (compared to background liver parenchyma). 3) Peritumoral irregular hyperenhancement in AP: existence of a visible portion adjacent to the lesion enhanced at the AP. 4) Peritumoral hypoenhancement in HBP: Peritumoral parenchymal enhancement with a wedge-shaped or bud-shaped protrusion in HBP. 5) Presence of capsule: thin uniform ring-like enhancement surrounding the tumor (which was different from that of the lesion or surrounding tissue) on the AP or HBP images. 6) Incomplete capsule: A certain area of the capsule is disrupted or even disappears. 7) In tratumoral homogeneity, "homogeneous" enhancement was defined as a whole and diffuse enhancement of the lesion, while "heterogeneous" enhancement was defined as the mixed enhancement of two or more enhancement echoes of the lesion.

2.5. Histopathologic Examination

A senior pathologist (X.L., working in the field of liver pathological diagnosis for 12 years) reviewed all surgical specimens to identify VETC patterns. The VETC pattern is defined as the presence of sinusoid-like vessels that form web-like networks and encapsulate individual tumor clusters on imaging with CD34 immunostaining (*21*). Cases with a visible VETC pattern in whole or part of the CD34 slides were identified as VETC positivity, and those without any VETC pattern were identified as VETC negativity (Figure 2).

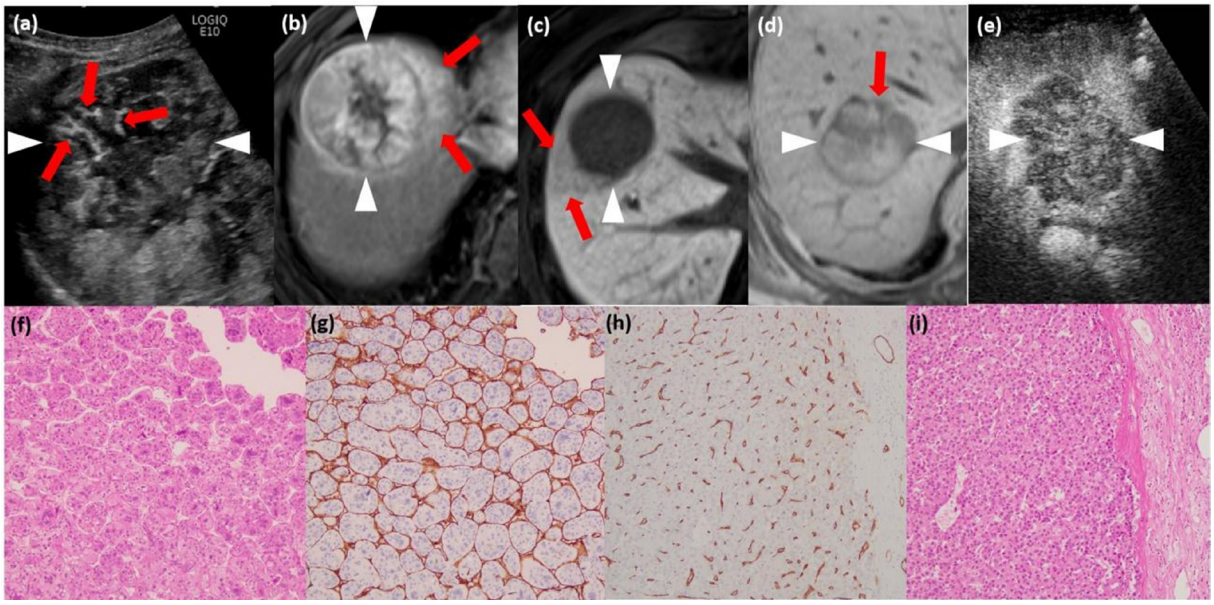

Figure 2. Typical imaging features and histological photos. (a) shows branching enhancement in AP of CEUS (arrow). **(b)** shows peritumoral hyperenhancement in AP of EOB-MRI (arrow) and intratumoral "heterogeneous" enhancement. **(c)** exhibit peritumoral hypoenhancement in HBP of EOB-MRI (arrow) and intratumoral "homogeneous" enhancement. **(d)** exhibit incomplete capsule of the lesion (arrow) and intratumoral "heterogeneous" enhancement in HBP of EOB-MRI. **(e)** shows irregular margin in PVP of CEUS and "heterogeneous" enhancement. Arrowheads in **(a)** to **(e)** represent the lesion. **(f)** and **(l)** are based on Hematoxylin & Eosin stain, while **(g)** and **(h)** are immunohistochemical staining for CD34. **(f–g)** are a case of VETC positive. **(h–l)** are another case of VETC negative. (Original magnifications x 100). For VETC positive lesion, endothelial cells envelope the HCC cell clusters and formed spider webs **(g)**, whereas VETC-negative lesion shows only sparse cord-like vessels **(h)**.

2.6. Survival analysis

Patients were followed up by telephone, outpatient visits, and rehospitalization. OS and progression-free survival (PFS) were defined as the interval from the date of operation to the date of last living visit or death and the date of recurrence, respectively. Recurrence was confirmed by CEUS, contrast-enhanced computed tomography (CECT), EOB-MRI, positron emission tomography (PET)-CT, and/or pathological diagnosis such as tumor biopsy. The endpoint for follow-up was March 31, 2024.

2.7. Statistical Analysis

The enumeration data between the VETC-positive and VETC-negative groups were calculated using the chi-square test. Non-normally distributed data are presented as medians and quartiles, and the Mann–Whitney *U* test was used to compare intergroup differences. Continuous variables that showed normal distribution were presented as mean ± standard deviation and compared using Student's *t*-test. The interobserver variability for radiological features was assessed using the *kappa* analysis (κ=0.00–0.20, poor agreement; κ=0.21–0.40, fair agreement; κ=0.41–0.60, moderate agreement; κ=0.61–0.80, good agreement; κ=0.81–1.0, excellent agreement). Baseline and survival data were analyzed on the basis of patients and non-lesions. When a patient has multiple HCC lesions, the patient is defined as VETC-positive if at least one lesion is VETC-positive. In contrast, the patient was defined as VETC-negative when all HCC lesions were negative for VETC. Univariate analysis was used to assess the significance of each variable in discriminating the presence of VETC in the training cohort. The selection method of best subset regression (BSR) was used to identify independent predictors and rule out potential confounding variables. The final nomogram model was developed. For the validation process, the receiver operator characteristic curve (ROC) was plotted, the area under the ROC curve (AUC) was estimated, and intergroup differences in the AUC were compared using the Delong test. Survival curves were plotted using the Kaplan-Meier method. Differences in PFS and OS were calculated using log-rank tests. All statistical analyses were performed using STATA 15.0, R 4.0.3, and MedCalc. Statistical significance was set $P < 0.05$.

3. Results

3.1. Baseline Characteristics

Baseline patient characteristics are summarized in Table 1. The 111 lesions included 87 VETC-negative and 24 VETC-positive. The incidence of VETC was 21.6% at the base of the lesion. The incidence of VETC was 20.8% (21/101) on patient base. The baseline patient characteristics are shown in Table 1. There were no statistical differences in demographic or serological indicators between the VETC-positive and VETC-negative groups.

Table 1. Demographic and serological characteristics of HCC patients[1,2]

	All *n*=101	VETC-positive *n* = 21	VETC-negative *n* = 80	*P* value[3]
Demographic characteristics				
Age ([median, Q], years)	69.0 (63.0, 75.0)	66.0 (63.0, 74.0)	69.0 (62.8, 75.2)	0.728
Gender (male/female)	81/20	17/4	64/16	1.000
Etiology (HCV/HBV/others[3])	11/47/43	1/11/9	10/36/34	0.688
Cirrhosis (No/Yes)	52/49	12/9	40/40	0.736
Serological characteristics				
AFP ([median, Q], mg/mL)	11.0 (4.00, 137)	11.0 (4.00,342)	11.5 (4.00.129)	0.546
Alb (x±s, g/dL)	4.18±0.51	4.31±0.58	4.14±0.48	0.211
T-BIL ([median, Q], mg/dL)	0.90 (0.70, 1.10)	0.90 (0.60, 1.40)	0.90 (0.70, 1.10)	0.493
PT-INR [median, Q)]	1.04 (0.97, 1.12)	1.02 (0.97, 1.12)	1.04 (0.98, 1.11)	0.700
Platelets ([median, Q], 10^{10}/L]	15.4 (10.7, 20.0)	15.6 (11.8, 23.9)	15.1 (10.6, 19.9)	0.610
PIVKA-II ([median, Q], mAU/mL)	94.0 (28.0, 629)	133 (35.0, 2020)	92.0 (28.0, 613)	0.467
ICG-R15 ([median, Q], %)	15.1 (10.4, 22.1)	12.9 (8.40, 18.9)	15.6 (11.0, 22.8)	0.175

[1]*Abbreviations*: HCC, Hepatocellular carcinoma; VETC, vessels encapsulating tumor clusters; HCV, hepatitis C virus; HBV, hepatitis B virus. AFP, alpha-fetoprotein; Alb, serum albumin; T-BIL, total bilirubin; PT, prothrombin time; INR, international normalized ratio; PIVKA-II, prothrombin induced by vitamin K absence II; ICG-R15: Indocyanine green 15 min retention. x±s: mean ±standard deviation; Q:1st quartile, 4th quartile. [2] The groupings of VETC and statistics in this table are based on patients. [3]"Others" included etiologies of alcoholic liver disease, non-HBV non-HCV, nonalcoholic steatohepatitis, and primary biliary cirrhosis.

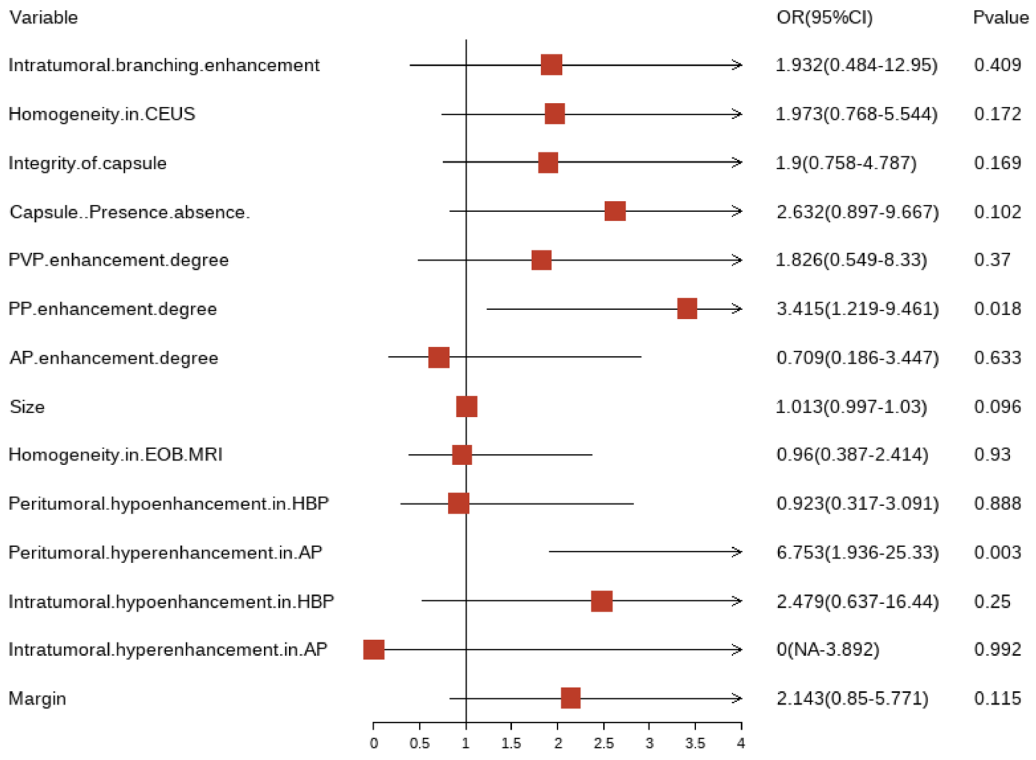

Figure 3. Forest plot demonstrating the univariate regression model for predicting VETC. Abbreviations: CEUS, contrast-enhanced ultrasound; AP, arterial phase; PP, portal phase; PVP, postvascular phase; HBP, hepatobiliary phase; EOB-MRI, magnetic-resonance imaging using gadolinium-ethoxybenzyl-diethylenetriamine penta-acetic acid; OR, odds ratio; VETC, vessels encapsulating tumor clusters.

3.2. Potential risk factors of VETC selection

The interobserver agreement for the radiological features indicated for the VETC patterns was good to excellent between the two doctors (F. W. and A.F.). The *kappa* values ranged from 0.663 to 0.955 (Table S1, *http://www.biosciencetrends.com/action/getSupplementalData.php?ID=203*).

As shown in Figure 3, an initial variable screening was first performed using univariate analysis. When selecting possible risk factors for establishing a clinical prediction model, the first step of univariate analysis cannot be based on $P < 0.05$ as a general statistical analysis. A typical entry criterion of *P*-value threshold should be relaxed (such as 0.15 (*22*), 0.2 (*23*), 0.25 (*24*)) to allow more factors that may be relevant to VETC to

Table 2. Final predictors for the risk of VETC in HCC patients[1]

Characteristics	Estimate	SE	Z	*P*	OR	VIF	Tolerance
(Intercept)	-7.666	1.952	-3.927	< 0.001	0.002		
Peritumoral hyperenhancement in AP (presence)	2.386	0.861	2.772	0.006	10.871	1.427	0.7006110
Peritumoral hypoenhancement in HBP (presence)	1.790	0.865	2.070	0.038	5.991	1.715	0.5830635
Size	0.023	0.012	1.874	0.061	1.023	1.570	0.6369370
Enhancement degree in PP (hypo)	1.393	0.613	2.274	0.023	4.027	1.080	0.9262363
Integrity of capsule (incomplete)	1.043	0.543	1.920	0.055	2.839	1.064	0.9394779
Intratumoral branching enhancement in CEUS (presence)	1.702	1.042	1.634	0.102	5.487	1.223	0.8169957

[1]*Abbreviations*: HCC, Hepatocellular carcinoma; AP, arterial phase; PP, portal phase; HBP, hepatobiliary phase; CEUS, contrast-enhanced ultrasound; SE, standard error; OR, odds ratio; VIF, variance inflation factor; VETC, vessels encapsulating tumor clusters. All VIF values were < 2.

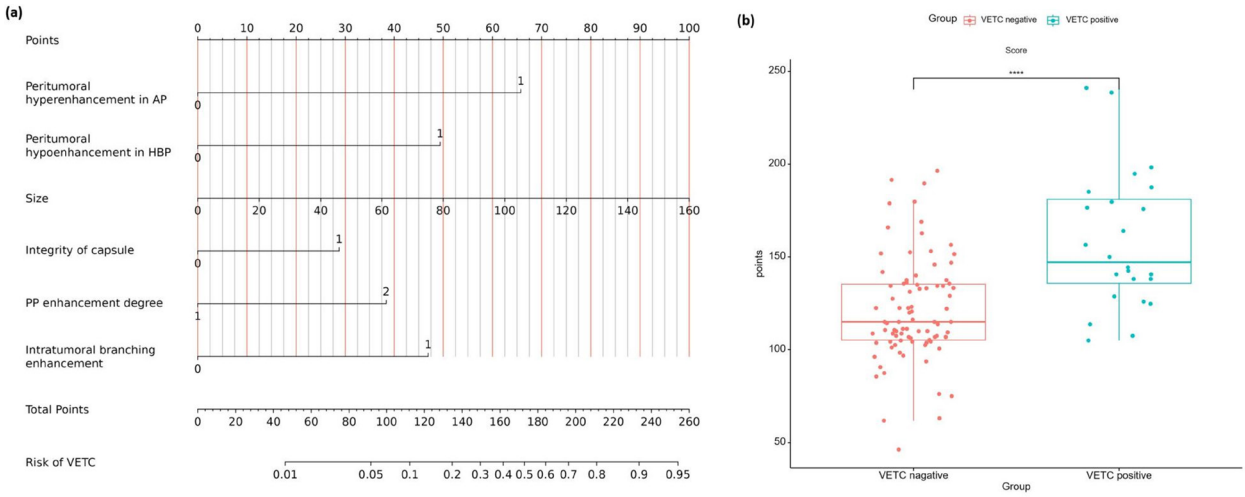

Figure 4. Nomogram and nomoscore for predicting the probability of VETC. (a) The constructed nomogram for predicting VETC. **(b)** A boxplot of nomoscore between VETC positive and negative group. Abbreviations: AP, arterial phase; HBP, hepatobiliary phase; PP, portal phase; VETC, vessels encapsulating tumor clusters.

enter subsequent screening. Therefore, the variables with a *P*-value of less than 0.2 (seven imaging features of "size," "margin," "capsule (presence/absence)," "integrity of capsule," "PP enhancement degree," "homogeneity in CEUS" and "peritumoral hyperenhancement in AP") were chosen for subsequent analysis. In addition, "peritumoral hypoenhancement in HBP" (*25*) has been considered a key aggressive imaging feature in published studies. SonoVue is a pure blood-pool contrast agent that does not enter the vascular space. Because the images of CEUS totally reflect intravascular contrast perfusion rather than stroma, we wanted to explore whether the spatial pattern of contrast-enhanced perfusion could reflect the pathological pattern of vascular encapsulation of VETC. Furthermore, some CEUS perfusion modes (such as "arterial enhancing modes with a fissure or flakiness style (*25*)," "fine network of many hyperenhancing lines" (*26*)) have been studied in HCC progression and invasion. After careful consideration, we included "peritumoral hypoenhancement in HBP" and "intratumoral branching enhancement," which yielded *P* value of more than 0.2, in the follow-up multivariate and BSR analysis. The "PP enhancement degree," "peritumoral hyperenhancement in AP," "branching enhancement," "integrity of capsule," "peritumoral hypoenhancement in HBP" and "size" were identified as effective sets of factors. Our final model with these six variables had an Akaike information criterion (AIC) of 106.4, the smallest AIC compared to a model with any other combination of factors (radiological features). No significant statistical collinearity was observed for any of the 6 variables (Table 2).

3.3. Development and presentation of the prediction model

Based on the findings of the above regression analysis, we obtained the following regression equation: Logit (*P*) = –7.666 + 2.386×"peritumoral hyperenhancement in AP" + 1.790×"peritumoral hypoenhancement in HBP" + 1.393×"PP enhancement degree" + 0.023×"size" + 1.043×"integrity of capsule" + 1.702×"branching enhancement."

The model was visualized in the form of a nomogram (Figure 4a). The nomogram included a preliminary score for each of the six predictors (ranging from 0 to 100). These scores were summed to obtain the total score (range, 0–260), which translates into the

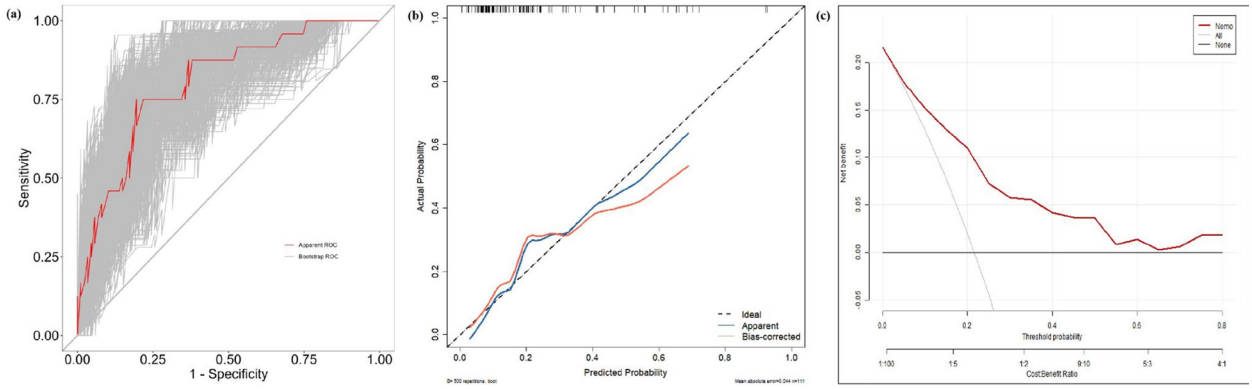

Figure 5. valuation and assessment of our model. (a) AUC by receiver operating characteristic curve (ROC) analysis by bootstrapping. Many of the gray curves are AUC made by repeated sampling 500 times. The red curve is the average AUC of 500 curves. **(b)** Calibration curves (blue curve is nomogram model while red curve is bootstrap validation). **(c)** Decision curve analysis (DCA). The DCA demonstrated that the threshold probability of the prediction model is approximately more than 5%.

individual probability (1–95%) of VETC for HCC lesions. For clinical application, according to the nomogram algorithm, the nomoscore was calculated for each lesion and plotted to assess risk stratification of the established nomogram (Figure 4b). For the VETC-negative and -positive lesion groups, the median (range) score values were 115 (46.3–196.4) and 147.5 (105.0–241.1), respectively. We observed a marked difference in the nomoscore profiles between the positive and VETC-negative groups ($P < 0.001$). The model is made available as an easy-to-use online calculator (*https://wangfeiqian126.shinyapps.io/dynnomapp/*) (Figure S1, *http://www.biosciencetrends.com/action/getSupplementalData.php?ID=203*).

3.4. Validation and assessment of model performance

The AUC of our nomogram model was 0.804 (95% confidence interval [CI], 0.707–0.901; $P < 0.05$; Figure S2 (*http://www.biosciencetrends.com/action/getSupplementalData.php?ID=203*). Logit (*P*) accuracy was 0.820. Sensitivity and specificity were 0.375 and 0.943, respectively. The Hosmer-Lemeshow test was used to evaluate the goodness-of-fit of the logistic regression model, and the results showed that the regression equation was highly matched ($\chi^2 = 5.7439$, df = 8, $P = 0.6759$). Decision curve analysis (DCA) revealed that using the nomogram to predict VETC would probably add more benefit than treating all or no patients (Figure 5).

Some published studies used bootstrapping as their only validation (*27-31*) as bootstrapping is an ideal internal validation method for smaller sample sizes or for larger numbers of candidate predictors (*32*). Because of the small sample size included in this study, all data were used for modeling without splitting the training and validation sets. Bootstrapping (500 bootstrap replicates) was performed in the internal validation phase of our model. The AUC and calibration curves with bootstrapping did not change much when compared with those of our model (Figure 5 a, b).

3.5. Comparison of EOB-MRI model, CEUS model and combined model

We built models using the total imaging features of EOB-MRI (seven factors) and CEUS (seven factors). Our multimodal model, which combined factors of EOB-MRI and CEUS (six selected factors), yielded a higher AUC (0.804) than the EOB-MRI model (0.767) and CEUS model (0.7) (Figure 6). However, there was no statistical difference between their AUCs (multimodal model *vs.* EOB-MRI model, $P = 0.3921$; multimodal model *vs.* CEUS model, $P = 0.0933$).

3.6. A novel nomogram-based prognostic risk assessment

The median follow-up duration of all the 101 patients was 60.3 months (range, 3.7–146.3 months). The median time to recurrence was 33.9 months (range: 1–143.4 months).

The 3-, 5-, and 8-year OS rates were lower in the VETC-positive group than in the VETC-negative group (69.2% *vs.* 88.0%, 62.6% *vs.*77.0%, and 42.4% *vs.* 65.1%, respectively; $P = 0.027$; Figure 7a). Similarly, the 1-, 3-, 5-, and 8-year PFS rates were lower in the VETC-positive group than in the VETC-negative group (61.9% *vs.* 73.6%, 40.4% *vs.* 64.1%, 26.9% *vs.* 43.6%, and 11.5% *vs.* 33.6%, respectively; $P = 0.041$; Figure 7b).

To further confirm the validity of our VETC-related nomogram for predicting prognosis, we stratified all 101 patients into two risk groups according to the nomoscore. They were low-risk group: 0 ≤ nomoscore ≤ 168; and high-risk group: nomoscore >168. Kaplan-Meier survival curves for OS and PFS in the two risk groups according to the nomoscore were plotted (Figure 7c, d), which showed an obvious grading ability based on our nomogram ($P < 0.05$). In other words, the prognosis would be good when the total score calculated

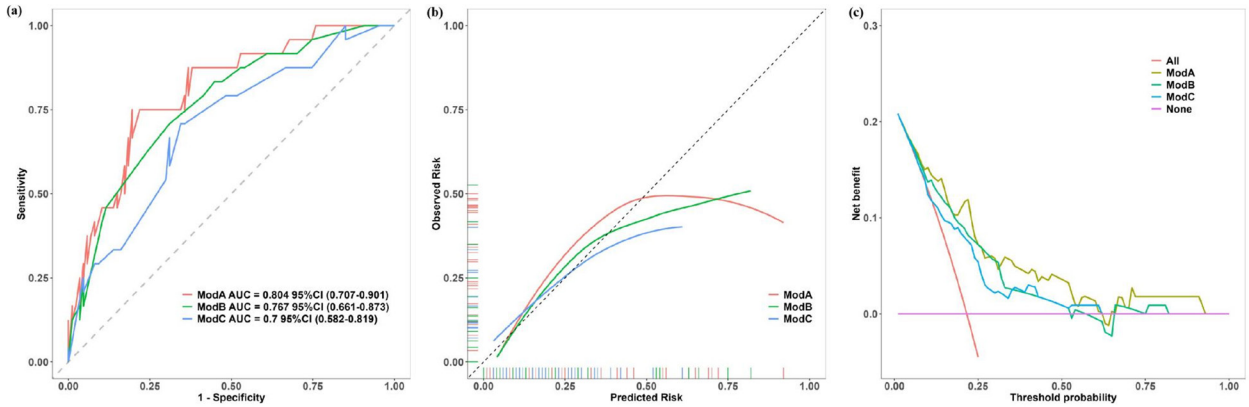

Figure 6. Comparison of three models. Model A is our final model with imaging factors of EOB-MRI and CEUS combined. Model B is EOB-MRI model. Model C is CEUS model. **(a)** AUC by receiver operating characteristic curve (ROC) analysis. Model A had the highest AUC. **(b)** Calibration curves. **(c)** Decision curve analysis (DCA). DCA showed that the nomogram that combined EOB-MRI and CEUS features had maximum clinical practicability. Abbreviations: HCC, Hepatocellular carcinoma; VETC, vessels encapsulating tumor clusters.

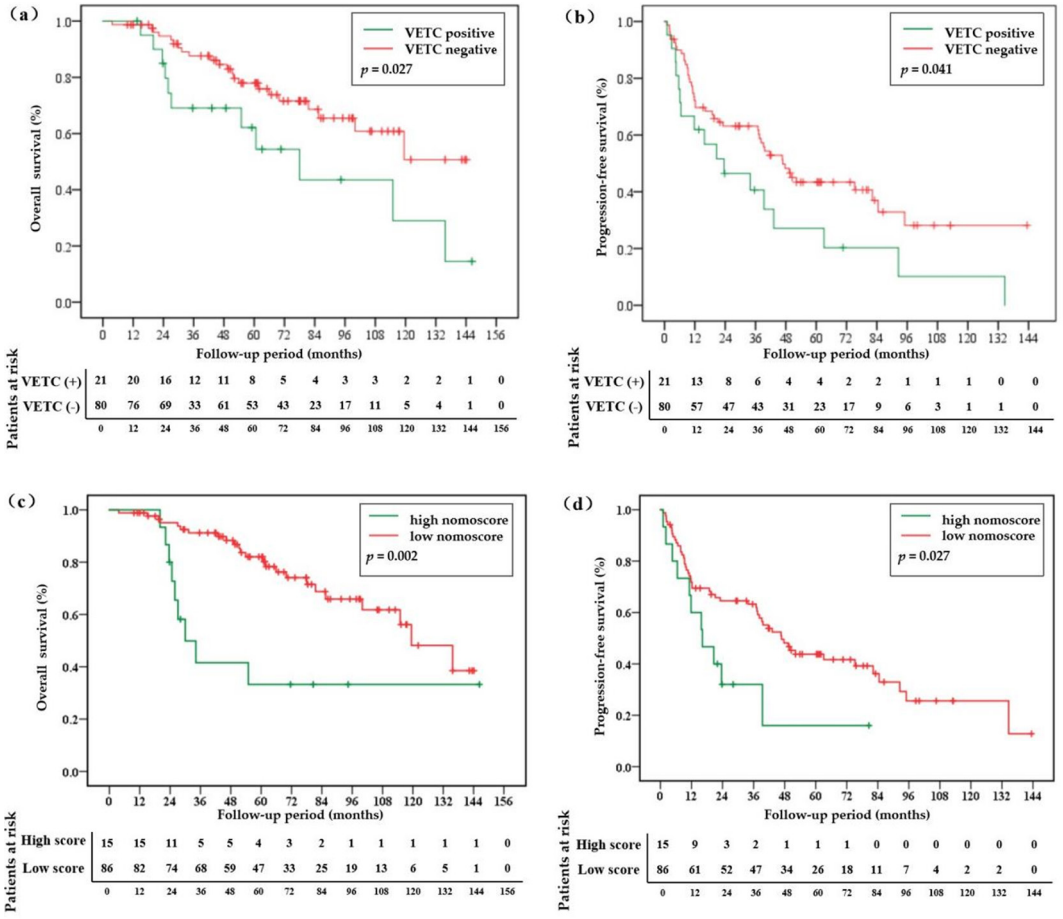

Figure 7. Survival rate curves of patients with HCC lesions of different VETC status and nomoscore risk stratification based on Kaplan-Meier survival analysis. OS **(a)** and PFS **(b)** are different between VETC positive and negative groups, with a p value of 0.027 and 0.041, respectively. According to our calculated nomoscore, OS **(c)** and PFS **(d)** among the low-risk and high-risk groups are different. Abbreviations: OS, Overall survival; PFS, Progression-free survival; HCC, Hepatocellular carcinoma; VETC, vessels encapsulating tumor clusters.

by "peritumoral hyperenhancement in AP," "peritumoral hypoenhancement in HBP," "PP enhancement degree," "size," "integrity of capsule" and "branching enhancement" was less than 168, but worse when the score was more than 168.

4. Discussion

Our study demonstrated that "size," "peritumoral hyperenhancement in AP," "peritumoral hypoenhancement in HBP," "integrity of the

capsule (incomplete)," "PP enhancement degree (hypoenhancement)," and "branching enhancement in AP of CEUS" can potentially predict VETC-positive HCC.

It is interesting that although VETC occurs within the lesion, peritumoral imaging features can predict VETC. Consistent with our findings, a published study showed that the peritumoral radiomics model yielded an incremental predictive value over the intratumoral model (AUC of peritumoral model=0.972, AUC of intratumoral model=0.919) (P = 0.044) (*14*). Abnormal peritumoral enhancement, regardless of AP or HBP, is widely recognized as a key independent risk factor for microvascular invasion (MVI) (*33*). MVI and VETC are the classical EMT-dependent and newly discovered EMT-independent patterns of hematogenous metastasis in HCC tumor cells, respectively (*3*). Regarding tumor behavior, for MVI, individual cancer cells separated from the primary site actively crossed the vessel wall and entered the vessel, while the tumor cluster passively was squeezed into the vessel in the VETC pattern. In short, tumor invasion and metastasis by the VETC pattern is simpler, easier, and more direct than MVI; thus, VETC has a higher invasive potential than MVI. MVI can be observed in up to 80% of VETC-positive tumors (*3*). Some researchers consider MVI and VETC to be synergistic (*34*). Therefore, it is not surprising that peritumoral imaging features, which are closely related to MVI, can predict VETC.

HCC lesions with the VETC pattern were found to have a higher intratumoral microvessel density than those without the VETC pattern (*35*). These blood vessels are considered to originate from tumor-associated dysplasia rather than from a normal vascular bed. Morphologically and structurally, tumor vasculature is characterized by dilated, tortuous, and disorganized blood vessels (*36*). They lack an endothelial basement membrane and form arteriovenous fistulas. These immature, unstable, and highly heterogeneous vessels have a high functional permeability (*36*). In this situation, the contrast agent is prone to rapid washout. Thus, one possible explanation for PP hypoenhancement is the large amount of abnormal angiogenesis in the VETC of HCC.

Previous studies have shown that large tumor size is related to VETC (*8,35*). As the tumor expands in size, the diffusion distance from the existing supplying vessels increases, leading to hypoxia. Hypoxia stimulates intratumoral vascular proliferation (*35*). As described below, increased intratumoral vessel density is closely related to VETC development. From this perspective, the correlation between tumor size and VETC suggests that tumor proliferation (an increase in lesion size on ultrasound images) may be one of the causes of VETC.

CEUS is the most sensitive tool for detecting intratumoral arterial vascularity (*11*). In agreement with our findings of branching enhancement in AP of CEUS, it was reported that HCC having VETC exhibits a "crack- and tendon-like filling" characteristic throughout the AP of CEUS until the contrast agent reaches its peak (*19*). Theoretically, the imageological branching enhancement during the AP of CEUS may reflect the microscopic pattern of the web-like vascular networks of VETC.

Tumor capsules, which we observed in the images, were mainly composed of fibroblasts and endothelial cells. They can act as barriers to the infiltration of peritumoral immune cells (*37*). However, Wu. R *et al*. found that the incomplete capsule of HCC lesions may result in reduced intratumoral spatial continuity of tumor cells and, through a complex mechanism, redistribution of peritumoral immune cells (*38*). Therefore, a radiologic incomplete capsule has been found to promote tumor invasion in many studies (*39*). VETC indicates that the cancer nests are surrounded, cut, and extruded by a network of blood vessels, which may suggest a discontinuity in the spatial structure of tumor cells. When VETC develops, the cancer cells are thought to easily escape from the immune response because genes representing effective immune responses are less enriched in the VETC positive group than in the negative group (*40*). These findings suggest that incomplete capsules may contribute to VETC and promote peritumoral invasion by altering tumor immunity.

Few VETC studies have combined CEUS with CEMRI. The choice of radiological modality (CT, US/CEUS, or MRI) depends on the patient, institutional, and regional factors (*41*). According to the HCC management guidelines of some countries, the diagnosis of HCC should be based on typical imaging features on at least two of the three imaging modalities, including contrast-enhanced computed tomography (CECT), MRI or EOB-MRI, and CEUS (*42*). However, some cases of pathologically early HCC are typically hypovascular and thus unlikely to be detected by CECT (*11*). Therefore, as 62% of HCC cases are in Barcelona Clinic Liver Cancer (BCLC) stages 0 and A in Japan (*43*), CEUS and EOB-MRI are the two main screening modalities for high-risk patients in Japan. In other words, both EOB-MRI and CEUS are routine preoperative examinations in Japan, with or without VETC evaluation. As some discrepancies were found between CEUS and EOB-MRI in evaluating the features of HCC (*44*), we believe the diagnostic strategy of their combination would be of great necessity. Furthermore, our study shows that the combination of EOB-MRI and CEUS has a better diagnostic effect on VETC according to all aspects we assessed (discrimination by AUC, calibration by Hosmer-Lemeshow analysis, and net benefit gain by DCA). Encouragingly, the combination of CEUS and EOB-MRI provides rich useful diagnostic information (VETC in our study, MVI (*45*), histological grade (*46*)) other than the diagnosis of HCC.

Consistent with some published VETC studies (*6,47*), our study also found that the presence of VETC had a long-term effect on survival. The VETC-positive and-negative groups had different OS and PFS. Thus, the

early diagnosis of VETC may be of great importance in predicting the prognosis of patients with HCC.

This study had some limitations. First, there was a potential for selection bias due to the retrospective nature of the study. Second, the sample size of this study was small and there was no external validation group to confirm the stability and applicability of the prediction model. Finally, the patients were all Japanese, with a relatively low incidence of VETC compared with published research in other countries (*3*). The results of our research are not representative of the situation in Asia or the world. Our study is the first multimodal imaging study to combine EOB-MRI and CEUS; in particular, we achieved excellent diagnostic efficiency. Therefore, we believe our study has important reference value for the preoperative diagnosis of VETC. More importantly, EOB-MRI and CEUS are routine liver cancer diagnostic and therapeutic steps implemented in accordance with liver cancer guidelines. These are not redundant diagnostic methods specifically added for the diagnosis of VETC. Therefore, real-world clinical work does not significantly increase the financial and time burden of patients and physicians. Furthermore, the visual and easy-to-use nomogram and nomoscore proposed in this paper can not only predict the VETC status of HCC lesions but also predict the survival condition of patients. The results of this study have great application prospects in clinical settings.

5. Conclusion

Combining CEUS and EOB-MRI, imaging features with peritumoral enhancement on AP and HBP of EOB-MRI, intratumoral branching enhancement in AP of CEUS, intratumoral hypoenhancement in PP of CEUS, incomplete capsule, and size show a satisfactory performance of VETC prediction in HCC. This study provides a promising approach for the noninvasive preoperative prediction of VETC using enhanced imaging.

Funding: This research was supported by the National Natural Science Foundation of China (No. 82102074) and Beijing Xisike Clinical Oncology Research Foundation of China (No. Y-Young2022-0162).

Conflict of Interest: The authors have no conflicts of interest to disclose.

References

1. Wen T, Jin C, Facciorusso A, Donadon M, *et al*. Multidisciplinary management of recurrent and metastatic hepatocellular carcinoma after resection: an international expert consensus. Hepatobiliary Surgery and Nutrition. 2018; 7: 353-371.
2. Lin YL, Li Y. Study on the hepatocellular carcinoma model with metastasis. Genes & Diseases. 2020; 7: 336-350.
3. Liu K, Dennis C, Prince DS, Marsh-Wakefield F, Santhakumar C, Gamble JR, Strasser SI, McCaughan GW. Vessels that encapsulate tumour clusters vascular pattern in hepatocellular carcinoma. JHEP Reports. 2023; 5:100792.
4. Wang JH, Li XS, Tang HS, Fang RY, Song JJ, Feng YL, Guan TP, Ruan Q, Wang J, Cui SZ. Vessels that encapsulate tumor clusters (VETC) pattern predicts the efficacy of adjuvant TACE in hepatocellular carcinoma. Journal of Cancer Research and Clinical Oncology. 2023; 149:4163-4172.
5. Lin W, Lu L, Zheng R, Yuan S, Li S, Ling Y, Wei W, Guo R. Vessels encapsulating tumor clusters: a novel efficacy predictor of hepatic arterial infusion chemotherapy in unresectable hepatocellular carcinoma. Journal of Cancer Research and Clinical Oncology. 2023; 149:17231-17239.
6. Dennis C, Prince DS, Moayed-Alaei L, Remash D, Carr-Boyd E, Bowen DG, Strasser SI, Crawford M, Pulitano C, Kench J, McCaughan GW, McKenzie C, Liu K. Association between vessels that encapsulate tumour clusters vascular pattern and hepatocellular carcinoma recurrence following liver transplantation. Frontiers in Oncology. 2022; 12:997093.
7. Fang JH, Xu L, Shang LR, Pan CZ, Ding J, Tang YQ, Liu H, Liu CX, Zheng JL, Zhang YJ, Zhou ZG, Xu J, Zheng LM, Chen MS, Zhuang SM. Vessels that encapsulate tumor clusters (VETC) pattern is a predictor of sorafenib benefit in patients with hepatocellular carcinoma. Hepatology. 2019; 70:824-839.
8. Renne SL, Woo HY, Allegra S, Rudini N, Yano H, Donadon M, Vigano L, Akiba J, Lee HS, Rhee H, Park YN, Roncalli M, Tommaso LD. Vessels encapsulating tumor clusters (VETC) is a powerful predictor of aggressive hepatocellular carcinoma. Hepatology. 2020; 71:183-195.
9. Kudo M. Breakthrough Imaging in Hepatocellular Carcinoma. Liver Cancer. 2016; 5: 47-54.
10. Wang F, Numata K, Nihonmatsu H, Okada M, Maeda S. Application of new ultrasound techniques for focal liver lesions. Journal of Medical Ultrasonics. 2020; 47:215-237.
11. Kudo M, Kawamura Y, Hasegawa K, Tateishi R, Kariyama K, Shiina S, Toyoda H, Imai Y, Hiraoka A, Ikeda M, *et al*. Management of hepatocellular carcinoma in Japan: JSH Consensus Statements and Recommendations 2021 Update. Liver Cancer. 2021; 10:181-223.
12. EASL Clinical Practice Guidelines: Management of hepatocellular carcinoma. Journal of Hepatology. 2018; 69:182-236.
13. General Office, N.H.C. Standard for diagnosis and treatment of primary liver cancer (2022 edition). Journal of Clinical Hepatology. 2022; 38:288-303.
14. Yu Y, Fan Y, Wang X, Zhu M, Hu M, Shi C, Hu C. Gd-EOB-DTPA-enhanced MRI radiomics to predict vessels encapsulating tumor clusters (VETC) and patient prognosis in hepatocellular carcinoma. European Radiology. 2022; 32:959-970.
15. Fan Y, Yu Y, Hu M, Wang X, Du M, Guo, L, Hu, C. Imaging features based on Gd-EOB-DTPA-enhanced MRI for predicting vessels encapsulating tumor clusters (VETC) in patients with hepatocellular carcinoma. The British Journal of Radiology. 2021; 94:20200950.
16. Hong SB, Choi SH, Kim SY, Shim JH, Lee SS, Byun JH, Park SH, Kim KW, Kim S, Lee NK. MRI features for predicting microvascular invasion of hepatocellular

carcinoma: A systematic review and meta-analysis. Liver Cancer. 2021; 10:94-106.
17. Wang F, Numata K, Chuma M, Miwa H, Moriya S, Ogushi K, Okada M, Otani M, Inayama Y, Maeda S. A study on the inconsistency of arterial phase hypervascularity detection between contrast-enhanced ultrasound using sonazoid and gadolinium-ethoxybenzyl-diethylenetriamine penta-acetic acid magnetic resonance imaging of hepatocellular carcinoma lesions. Journal of Medical Ultrasonics. 2021; 48:215-224.
18. Xu W, Huang B, Zhang R, Zhong X, Zhou W, Zhuang S, Xie X, Fang J, Xu M. Diagnostic and prognostic ability of contrast-enhanced unltrasound and biomarkers in hepatocellular carcinoma subtypes. Ultrasound in Medicine and Biology. 2024; 50:617-626.
19. Lan CY, Ling B, Guo WW, Yin W, Zhong XG, Han YM, Dong XF. The relationship between vimentin protein expression in endothelial cells and contrast-enhanced ultrasound characters in VETC (+) hepatocellular carcinoma. Zhonghua Zhong Liu Za Zhi. 2018; 40:105-109. (in Chinese).
20. Van der Horst G, Buijs JT, Van der Pluijm G. Pre-clinical molecular imaging of "the seed and the soil" in bone metastasis. In Bone Cancer, Elsevier. 2015;557-570.
21. Lee W, Lam S, Zhang Y, Yang R, Cai J. Review of methodological workflow, interpretation and limitations of nomogram application in cancer study. Radiation Medicine and Protection. 2022; 3:200-207.
22. Yang K, Xie W, Zhang X, Wang Y, Shou A, Wang Q, Tian J, Yang J, Li G. A nomogram for predicting late radiation-induced xerostomia among locoregionally advanced nasopharyngeal carcinoma in intensity modulated radiation therapy era. Aging (Albany NY). 2021; 13:18645-18657.
23. Dong N, Wang S, Li X, Li W, Gao N, Pang L, Xing J. Prognostic nomogram for the severity of acute organophosphate insecticide self-poisoning: a retrospective observational cohort study. BMJ Open. 2021; 11:e42765.
24. Guner R, Kayaaslan B, Hasanoglu I, *et al*. Development and validation of nomogram to predict severe illness requiring intensive care follow up in hospitalized COVID-19 cases. BMC Infectious Diseases. 2021; 21:1004.
25. Zhang L, Yu X, Wei W, Pan X, Lu L, Xia J, Zheng W, Jia N, Huo L. Prediction of HCC microvascular invasion with gadobenate-enhanced MRI: correlation with pathology. European Radiology. 2020; 30:5327-5336.
26. Giorgio A, Calisti G, Di Sarno A, Farella N, De Stefano G, Scognamiglio U, Giorgio V. Characterization of dysplastic nodules, early hepatocellular carcinoma and progressed hepatocellular carcinoma in cirrhosis with contrast-enhanced ultrasound. Anticancer Research. 2011; 31:3977-3982.
27. Xie W, Liu M, Okoli C, Zeng L, Huang S, Ye X, Liu F, Wang J. Construction and evaluation of a predictive model for compassion fatigue among emergency department nurses: A cross-sectional study. International Journal of Nursing Studies. 2023; 148:104613.
28. Liang W, Zhang K, Cui J, Xi H, Cai A, Li J, Liu Y, Liu J, Zhang W, Wang P, Wei B, Chen L. Nomogram to predict prolonged postoperative ileus after gastrectomy in gastric cancer. World Journal of Gastroenterology. 2019; 25:5838-5849.
29. Ding N, Zhang J, Wang P, Wang F. A novel machine learning model for predicting clinical pregnancy after laparoscopic tubal anastomosis. BMC Pregnancy Childbirth. 2023; 23:537.
30. Van Straalen JW, Giancane G, Amazrhar Y, *et al*. A clinical prediction model for estimating the risk of developing uveitis in patients with juvenile idiopathic arthritis. Rheumatology (Oxford). 2021; 60:2896-2905.
31. Jatuworapruk K, Grainger R, Dalbeth N, Taylor WJ. Development of a prediction model for inpatient gout flares in people with comorbid gout. Annals of the Rheumatic Diseases. 2020; 79:418-423.
32. Shipe ME, Deppen SA, Farjah F, Grogan E.L. Developing prediction models for clinical use using logistic regression: an overview. Journal of Thoracic Disease. 2019; 11:S574-S584.
33. Hu F, Zhang Y, Li M, Liu C, Zhang H, Li X, Liu S, Hu X, Wang J. Preoperative Prediction of Microvascular Invasion Risk Grades in Hepatocellular Carcinoma Based on Tumor and Peritumor Dual-Region Radiomics Signatures. Frontiers in Oncology. 2022; 12:853336.
34. Qu Q, Liu Z, Lu M, Xu L, Zhang J, Liu M, Jiang J, Gu C, Ma Q, Huang A, Zhang X, Zhang T. Preoperative Gadoxetic Acid-Enhanced MRI Features for Evaluation of Vessels Encapsulating Tumor Clusters and Microvascular Invasion in Hepatocellular Carcinoma: Creating Nomograms for Risk Assessment. Journal of Magnetic Resonance Imaging. 2023 (Online ahead of print).
35. Huang CW, Lin SE, Huang SF, Yu MC, Tang JH, Tsai CN, Hsu HY. The vessels that encapsulate tumor clusters (VETC) pattern is a poor prognosis factor in patients with hepatocellular carcinoma: an analysis of microvessel density. Cancers (Basel). 2022; 14:5428.
36. Taskaeva I, Bgatova N. Microvasculature in hepatocellular carcinoma: an ultrastructural study. Microvascular Research. 2021; 133, 104094.
37. Rahmanzade R. Redefinition of tumor capsule: Rho-dependent clustering of cancer-associated fibroblasts in favor of tensional homeostasis. Medical Hypotheses. 2020; 135, 109425.
38. Wu R, Guo W, Qiu X, *et al*. Comprehensive analysis of spatial architecture in primary liver cancer. Science Advances. 2021; 7:g3750.
39. Zhu F, Yang F, Li J, Chen W, Yang W. Incomplete tumor capsule on preoperative imaging reveals microvascular invasion in hepatocellular carcinoma: a systematic review and meta-analysis. Abdominal Radiology. 2019; 44:3049-3057.
40. Zhang P, Ono A, Fujii Y, *et al*. The presence of vessels encapsulating tumor clusters is associated with an immunosuppressive tumor microenvironment in hepatocellular carcinoma. International Journal of Cancer. 2022; 151:2278-2290.
41. Granata V, Grassi R, Fusco R, Belli A, Cutolo C, Pradella S, Grazzini G, La Porta M, Brunese MC, De Muzio F, Ottaiano A, Avallone A, Izzo F, Petrillo A. Diagnostic evaluation and ablation treatments assessment in hepatocellular carcinoma. Infectious Agents and Cancer. 2021; 16:53.
42. Cho Y, Kim BH, Park JW. Overview of Asian clinical practice guidelines for the management of hepatocellular carcinoma: an Asian perspective comparison. Clinical and Molecular Hepatology. 2023; 29:252-262.
43. Kudo, M. Management of hepatocellular carcinoma in Japan as a world-leading model. Liver Cancer. 2018; 7:134-147.
44. Yang J, Jiang H, Xie K, Bashir MR, Wan H, Huang J, Qin Y, Chen J, Lu Q, Song B. Profiling hepatocellular carcinoma

aggressiveness with contrast-enhanced ultrasound and gadoxetate disodium-enhanced MRI: an intra-individual comparative study based on the Liver Imaging Reporting and Data System. European Journal of Radiology. 2022; 154:110397.
45. Zheng R, Zhang X, Liu B, Zhang Y, Shen H, Xie X, Li S, Huang G. Comparison of non-radiomics imaging features and radiomics models based on contrast-enhanced ultrasound and Gd-EOB-DTPA-enhanced MRI for predicting microvascular invasion in hepatocellular carcinoma within 5 cm. European Radiology. 2023; 33:6462-6472.
46. Wang F, Numata K, Nakano M, Tanabe M, Chuma M, Nihonmatsu H, Nozaki A, Ogushi K, Luo W, Ruan L, Okada M, Otani M, Inayama Y, Maeda S. Diagnostic value of imaging methods in the histological four grading of hepatocellular carcinoma. Diagnostics (Basel). 2020; 10:321.
47. Kawasaki J, Toshima T, Yoshizumi T, Itoh S, Mano Y, Wang H, Iseda N, Harada N, Oda Y, Mori M. Prognostic impact of vessels that encapsulate tumor cluster (VETC) in patients who underwent liver transplantation for hepatocellular carcinoma. Annals of Surgical Oncology. 2021; 28:8186-8195.

Received May 2, 2024; Revised June 2, 2024; Accepted June 7, 2024.

*Address correspondence to:
Kazushi Numata, Gastroenterological Center, Yokohama City University Medical Center, 4-57 Urafune-cho, Minami-ku, Yokohama, Kanagawa 232-0024, Japan.
E-mail: kz-numa@urahp.yokohama-cu.ac.jp

Released online in J-STAGE as advance publication June 12, 2024.